Direct stereotactic targeting of the ventrointermediate nucleus of the thalamus based on anatomic 1.5-T MRI mapping with a white matter attenuated inversion recovery (WAIR) sequence

François Vassal, Jérôme Coste, Philippe Derost, Vivien Mendes, Jean Gabrillargues, Christophe Nuti, Franck Durif, Jean-Jacques Lemaire

Direct stereotactic targeting of the ventrointermediate nucleus of the thalamus based on anatomic 1.5-T MRI mapping with a white matter attenuated inversion recovery (WAIR) sequence

François Vassal [a,b,*], Jérôme Coste[b], Philippe Derost[c], Vivien Mendes[b,d], Jean Gabrillargues[b,e], Christophe Nuti[a], Franck Durif[b,c], Jean-Jacques Lemaire[b,d]

[a] Neurosurgery Service, Centre Hospitalier Universitaire de Saint-Etienne, Hôpital Nord, 42270 Saint-Priest en Jarez, France

[b] Image-Guided Clinical Neurosciences and Connectomics, IGCNC, EA 3295, Equipe de recherche en signal et imagerie médicale, Université d'Auvergne, BP 10448, F-63000 Clermont-Ferrand, France

[c] Neurology Service, Centre Hospitalier Universitaire de Clermont-Ferrand, Hôpital Gabriel Montpied, F-63003 Clermont-Ferrand, France

[d] Neurosurgery Service, Centre Hospitalier Universitaire de Clermont-Ferrand, Hôpital Gabriel Montpied, F-63003 Clermont-Ferrand, France

[e] Neuroradiology Unit, Centre Hospitalier Universitaire de Clermont-Ferrand, Hôpital Gabriel Montpied, F-63003 Clermont-Ferrand, France

* Corresponding autor Tel.:+33 477 127 723; fax:+33 477 120 544. E-mail address: francoisvassal@wanadoo.fr (F. Vassal).

Abstract

Background

The ventrointermediate nucleus (Vim) of the thalamus is still considered "invisible" on current magnetic resonance imaging (MRI), requiring indirect methods based on stereotactic atlases for estimation of its location. Direct visualization of Vim is desirable to improve targeting.

Objective

To evaluate the ability of Inversion-Recovery 1.5-T MR images to produce high-resolution, anatomical depiction of the thalamus suitable for direct Vim targeting.

Methods

Twenty patients with essential tremor or tremor associated with Parkinson's disease received Vim deep brain stimulation (DBS). Fahn-Tolosa-Marin and Unified Parkinson's Disease Rating Scale (UPDRS) tremor scores were assessed pre- and postoperatively. Preoperative stereotactic 1.5-T MR images of the thalamus were acquired using a White Matter Attenuated Inversion Recovery (WAIR) sequence. Thalamic nuclei were manually contoured on the basis of spontaneous MRI contrasts; labeling relied on 3D identification from stereotactic books and in-house ex vivo 4.7-T microscopic MRI atlas. Vim was then directly probed for electrophysiological confirmation and determination of the optimal site for electrode placement.

Results

The shape, spatial orientation, and signal contrast of Vim as depicted on our WAIR images were similar to those observed on the Schaltenbrand and Bailey atlas, as well as in our high-field MRI atlas. These images were successfully used for pure direct Vim targeting: at the last follow-up (median = 46.3 months), the average tremor score improved from 3.80 preoperatively to 0.50 postoperatively (on stimulation; $P < 0.01$).

Conclusion

1.5-T MRI with WAIR sequence provides high-quality images of Vim suitable in DBS surgery, for accurate preoperative planning, direct targeting and anatomic analysis.

Introduction

The ventrolateral, motor area of the thalamus has been the prime target for stereotactic surgery of medically intractable tremor since the early 1950s [1]. The target of choice for tremor reduction has been shown to be the thalamic relay of vestibular and proprioceptive muscle spindle afferents [2,3], namely, the ventrointermediate nucleus (Vim), according to Hassler [4], or the ventral and posterior part of the ventral lateral posterior (VLp) nucleus (receiving cerebellar afferents), according to Hirai and Jones [5]. In the modern era, radiofrequency thalamotomy or chronic high-frequency stimulation of Vim have proven to be effective in up to 70% of tremor-disabled patients [6].

Vim is still reputed to be "invisible" on routinely available imaging techniques [7], and its indirect targeting remains the "gold standard". Various methods can be used to estimate its location. Most involve stereotactic atlases and preexisting data obtained by authors with considerable experience in the field of thalamotomy or thalamic deep brain stimulation (DBS) [8,9]. The coordinates are given by extrapolation, measuring distances from recognizable landmarks, such as the anterior (AC) and posterior (PC) commissures, and the thalamus height (TH). These landmarks can be located on ventriculography [1], computerized tomography (CT) [10], or magnetic resonance imaging (MRI) [11]. Coordinates are deduced using a human brain atlas or proportional geometric schemes, hypothesizing that the proportions are applicable to any individual. Other authors advocate direct visualization of anatomical structures bordering the motor thalamus nuclei, such as the internal capsule and the wall of the third ventricle [12].

One major concern with indirect targeting is the lack of precision inherent to the technique, as it does not take into account the interindividual variability of brain sizes [13,14] and the possible asymmetry between the two hemispheres of the same individual [3]. Hence, the method used for target location is intrinsically probabilistic. To compensate for this limited accuracy, many groups have developed electrophysiological methods aimed at the recognition of specific discharge patterns to optimally place the electrode within Vim [8]. This approach exposes the patient to additional risks related to the multiple cerebral tracts necessary to obtain physiologic assessments. Therefore, direct visualization of Vim appears desirable to improve the accuracy of target selection and reduce the number of brain penetrations.

Given recent advances in medical imaging, it became evident that direct visualization of structures invisible in the past was only a matter of time. Nowadays, common targets for functional stereotactic neurosurgery (such as the subthalamic nucleus (STN) and the internal globus pallidum (GPi)) are reliably identified and directly targeted (i.e., without atlas reference) with conventional MRI [3,15–17]. However, currently, inadequate image resolution and contrast preclude the use of an anatomic image-based targeting for Vim [7].

Recently, high-field MR imagers and modern MR sequences have gained wide acceptance as important tools in clinical and research studies [15,16,18–20]. The improved signal-to-noise ratio (SNR) and the possibility to benefit from spontaneous contrasts between white and gray matter signals can aid the identification of subtle structural features, with good geometric resolution. Based on our experience on MRI anatomic mapping [15,16,19,20], we have introduced a modification to the previously described Cortex Attenuated Inversion Recovery sequence [17], named White matter Attenuated Inversion Recovery (WAIR). We found that images generated by this sequence result in a consistent delineation of the ventral group of thalamic nuclei and the fiber projections reaching them from the basal ganglia as well as the cerebellar and lemniscal pathways. In this study, we reported the use of 1.5-T MRI with WAIR sequence to produce high-resolution, anatomical images of Vim suitable for stereotactic targeting. To assess the precision of direct visualization and targeting of Vim and its neighborhood during stereotactic neurosurgery, we retrospectively analyzed data collected in a consecutive series of patients treated by thalamic DBS surgery for disabling tremor.

Methods and materials

Population of patients

A consecutive series of 20 patients (14 males) with Parkinson's disease (PD, 13 cases) or essential tremor (ET, 7 cases) received unilateral (n = 8) or bilateral (n = 12) Vim DBS between May 2002 and December 2009. Their mean age was 62.5 ± 15.5 years (range, 27–79 years). All patients suffered from disabling tremor despite adequate pharmacological treatment. Patients were included in this study if they had a tremor score ≥3 on the pre-DBS Unified Parkinson Disease Rating Scale (UPDRS) Part III tremor item 21 [21] or Fahn-Tolosa-Marin clinical tremor rating scale (TRS) [22]. The average follow-up period was 46.3 ± 28.7 months (range, 8–86 months).

Targeting based on MRI and surgical procedure

In the operating room, a stereotactic frame (Leksell G frame, Elekta, Sweden) was secured to the patient's head with its repositioning kit (Leksell repositioning kit, Elekta, Sweden) after local anesthesia was administered. A stereotactic MRI was then performed (Sonata, 1.5-T, Siemens, Germany): WAIR sequence [14]; coronal plan (2D sequence); Repetition Time = 4500 ms; Echo Time = 13 ms; Inversion Time = 160 ms; 2 × 15 images (two interleaved series); acquisition = 2 × 9 min 33 s; voxel size = $0.52 \times 0.62 \times 2$ mm^3. Before anatomic mapping and trajectory planning, the stereotactic frame was removed for patient comfort. Anatomic labeling relied on 3D location adapted from anatomic and stereotactic books (Talairach and Tournoux [23], Schaltenbrand and Bailey [24], Morel and Magnin [25]) and in-house microscopic 4.7-T MRI atlas [20] allowing accurate 3D multiplanar analysis (Fig. 1). Vim and its anatomic neighbors were manually outlined according to spontaneous MRI contrasts; Vim was identified as a hypointense band crossing the ventrolateral thalamus, on coronal images (Fig. 2).
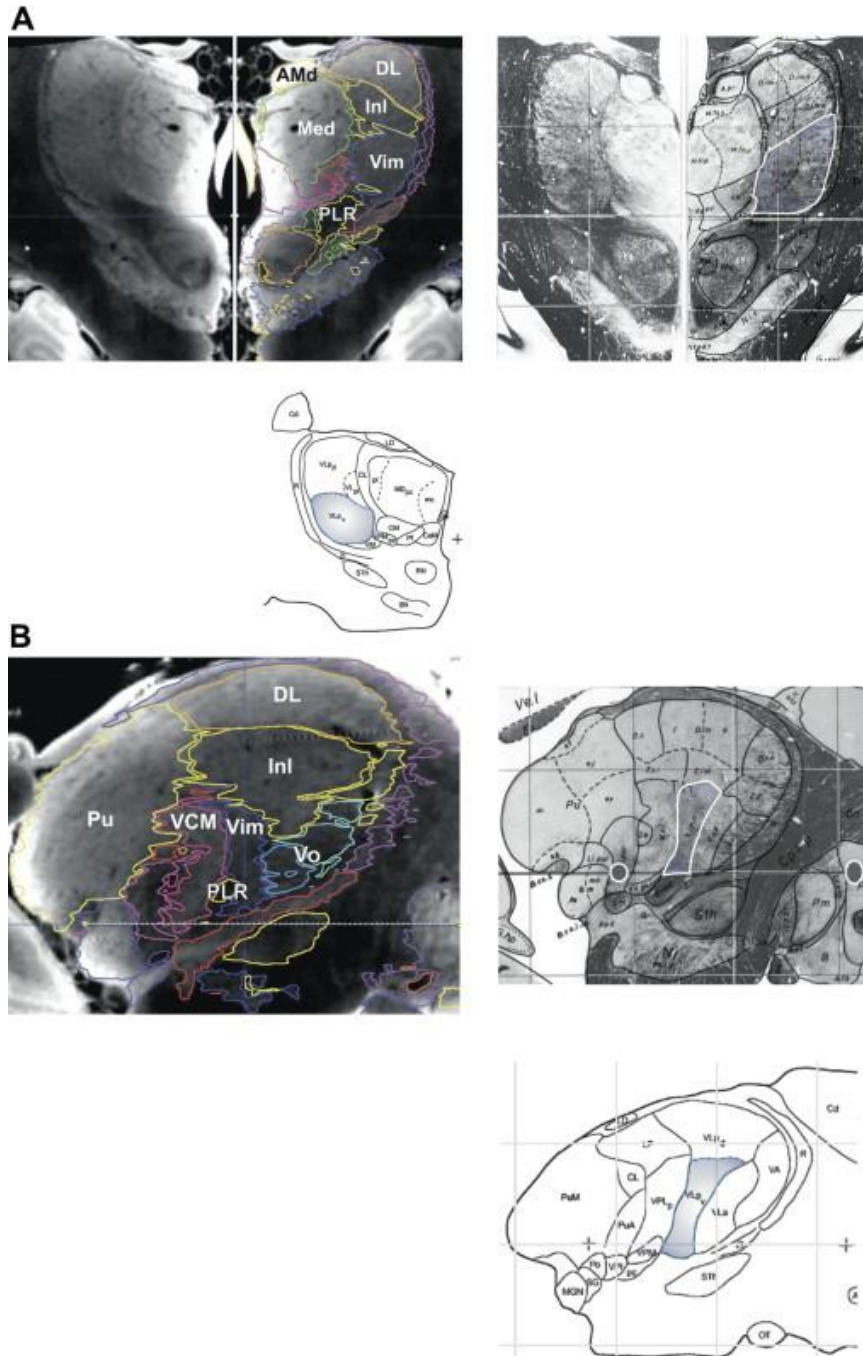
Figure 1. Anatomic aid used for preoperative planning; the ventrointermediate nucleus (Vim) is in blue: in-house ex vivo 4.7-T MRI [20] and equivalent sections in current stereotactic atlases (Morel et al. [25] [Mo] and Schaltenbrand and Bailey [24] [S&B]). (A) 4.7-T MRI coronal slice (top left; left without overlay of tracings) going through Vim; S&B's atlas (top right; 5 mm posteriorly to the inter-commissural midpoint; left without overlay of tracings) and Morel et al. atlas (bottom; 9 mm anteriorly to PC) sections. (B) 4.7-T MRI sagittal slice (top left), S&B's atlas (top right; 13.5 mm of laterality) and Mo's atlas (bottom; 13.5 mm of laterality) sections. AMd, nucleus anteromedial; Inl, nucleus intermediolateral; DL, nucleus dorsolateral; Med, nucleus medial; VCL, nucleus ventrocaudal lateral; VCM, nucleus ventrocaudal medial; Vo, nucleus ventro-oral; PLR, prelemniscal radiations; Pu, pulvinar; see Table 1 for terminology.
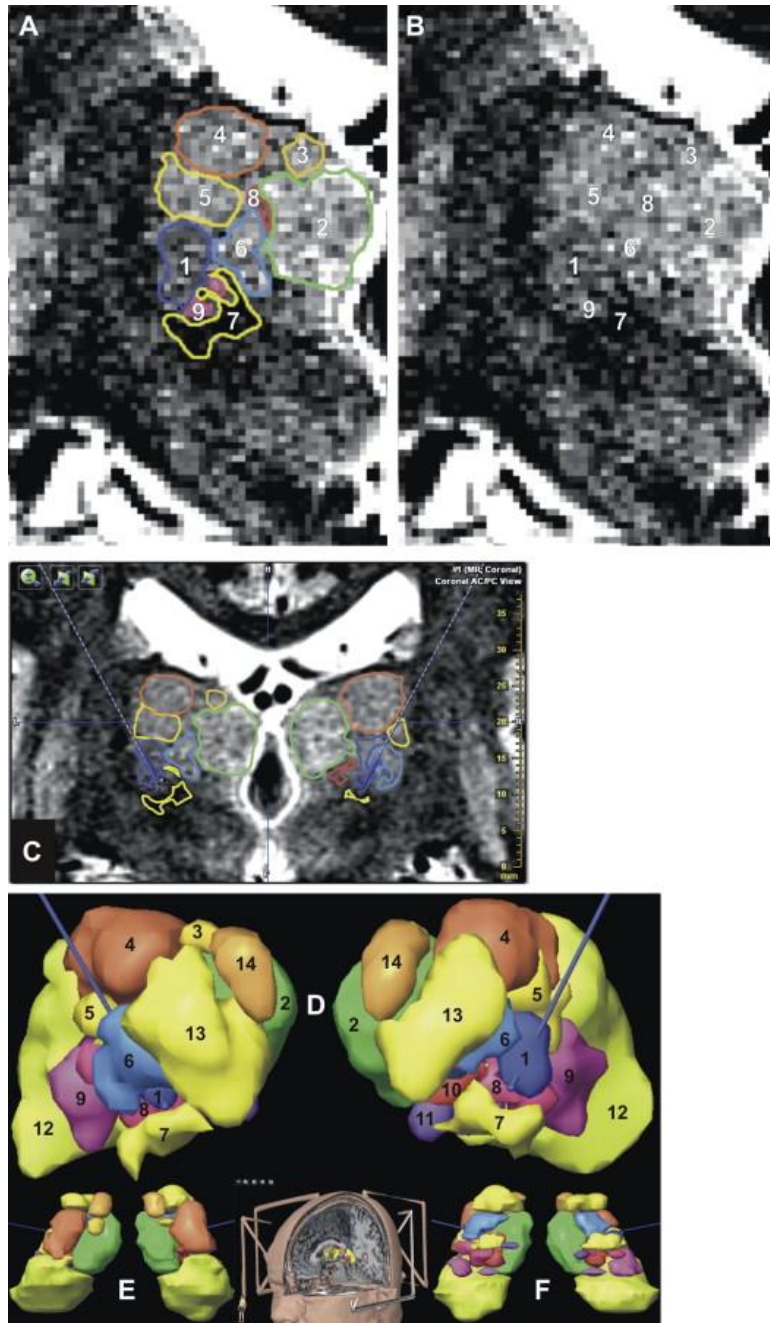
Figure 2. *3D stereotactic planning for targeting of the ventrointermediate nucleus (Vim), after manual outlining of thalamic nuclei (iPlan, BrainLab, Germany); from (A) to (F), same patient: (A) manual outlining of thalamic nuclei according to anatomic location and MRI contrasts on coronal MRI slice (White Matter Attenuated Inversion Recovery sequence, WAIR, voxel = 0.52 × 0.62 × 2 mm3, stereotactic frame and location box in place; 1.5-T, Siemens Sonata, Germany), the display is not interpolated in order to show the raw data; (B) same image, without outline; (C) Example of interpolated coronal stereotactic image with the right and left trajectories (dotted lines when projected and bold line when the trajectories cross the image); to facilitate the 3D positioning of trajectories, the outlines are displayed; (D) Frontal, (E) superior, (F) inferior views of 3D reconstruction of nuclei after manual outlining; (1) Vim, (2) nucleus medial, (3) nucleus dorsomedial, (4) nucleus dorsolateral, (5) nucleus intermediate, (6) nucleus ventro-oral, (7) prelemniscal radiations or prerubral field of Forel, (8) nucleus ventrocaudal medial, (9) nucleus ventrocaudal lateral, (10) nucleus center median, (11) nucleus parafascicular, (12) pulvinar, (13) nucleus anterolateral, (14) nucleus anteromedial; see **Table 1** for terminology.*

The endpoint of the trajectory was placed at the lower portion of Vim according to its known transversal somatotopy: the face, the upper limb and the lower limb, respectively from medial to lateral [1,8]. The x, y, and z coordinates were automatically calculated using dedicated software (iPlan, BrainLab, Germany). Double obliquity trajectory was optimized in order to explore Vim along its superior-inferior axis.

The following day, in the operating room, the stereotactic frame was repositioned under local anesthesia. The stereotactic electrode-guiding device was installed and a 6-mm burr hole was made at the level of the predetermined trajectory. If needed, two quadripolar electrodes (DBS 3389, Medtronic, USA) were placed (one per hemisphere) during the same procedure. For each electrode, we optimized the positioning of one contact (we always selected the contact n°1, located just above the distal one or contact n°0). Each DBS electrode was implanted after electrophysiological mapping with two exploration electrodes (Alpha Omega, Israel): one on the planned tract (named central), and one on a parallel additional tract situated 2 mm anteriorly (named anterior), or 2 mm medially (named medial). The electrophysiological analysis was performed along the distal 10 mm of tracts, from proximal to distal. We first recorded the spontaneous and evoked (passive joints movements) extracellular multiunit neuronal activity every 0.5 mm using the recording tip of the exploration electrode. Then, after retraction of the recording tip and moving out to −10 mm position, acute stimulation tests up to 3 mA were done every 1 mm. At each checkpoint, the clinical benefit and the adverse effects were recorded while increasing the stimulation current (step = 0.2 mA). The current thresholds linked to the clinical benefit and to adverse effects were noticed as well as the difference between the adverse effect threshold and the benefit threshold, named the stimulation margin. The DBS electrode was placed on the tract where we found the best stimulation parameters, the lowest benefit threshold with a high stimulation margin, without reference to extracellular multiunit neuronal activity. We systematically calculated the distance (mm) between the endpoint of the trajectory (lower border of Vim) and the optimal position determined intraoperatively: a positive value meaning a position above the lower border of Vim. Few days after, electrodes were connected to a programmable neurostimulator (Kinetra, Medtronic, USA).

Postoperative documentation of DBS electrode location

We analyzed DBS electrode location using postoperative radiographic control performed at the end of the surgical procedure: x-ray with stereotactic frame, at the beginning of the series, then CT without stereotactic frame. The coordinates of the center of the "effective" contact (i.e., used for chronic high-frequency DBS determined during the clinical follow-up) were calculated as follows: direct measurement of the stereotactic frame coordinates of the contact center on stereotactic x-rays, then display of this point within the preoperative stereotactic MRI; co-registration between preoperative MRI and postoperative CT-scan using mutual information algorithm (iPlan, BrainLAB, Germany) (Fig. 3) and contact location based on electrode artifact [26].
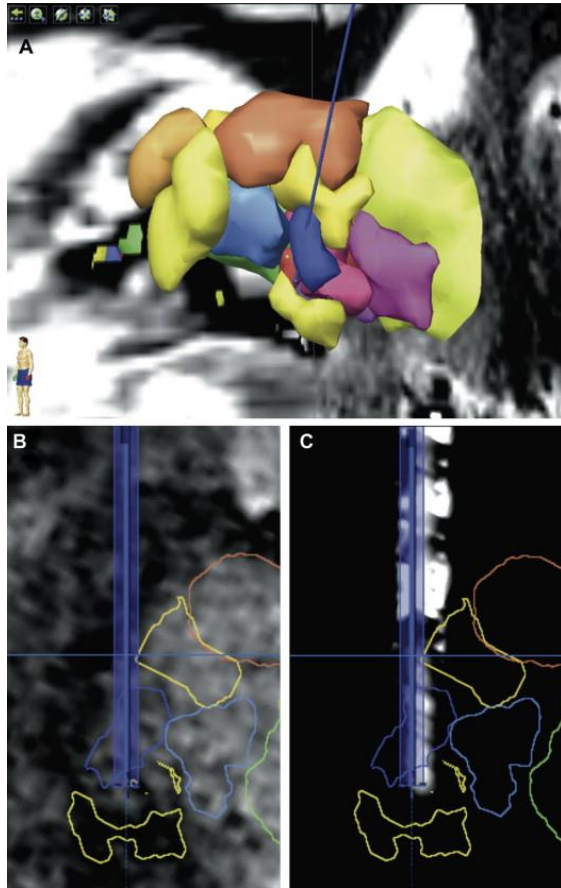
*Figure 3. Reconstructed images along the planned trajectory (left hemisphere, same patient than **Fig. 2,** same color code): (A) 3D anterolateral view showing the left trajectory (blue) going through the nucleus ventrointermediate (Vim, dark blue); (B) reconstructed MRI (WAIR sequence) slice along the planned trajectory; (C) reconstructed CT slice along the planned trajectory after co-registration (iPlan, BrainLab, Germany) of postoperative CT-scan (General Electric Discovery CT 750 HD, USA) with preoperative MRI data set; note the visibility of the distal four-contact zone of the DBS electrode within Vim.*

The locations of effective contacts were determined relatively to Vim contours defined on preoperative WAIR imaging. From contact locations displayed on preoperative stereotactic MRI, we also computed the relative coordinates in the proportional geometric scheme of Guiot et al. [9] modified by Benabid et al. [7] based on the AC-PC reference system (Fig. 4): laterality in mm, superior-inferior location in eighths of thalamus height, and anterior position from PC in twelfths of AC-PC line.
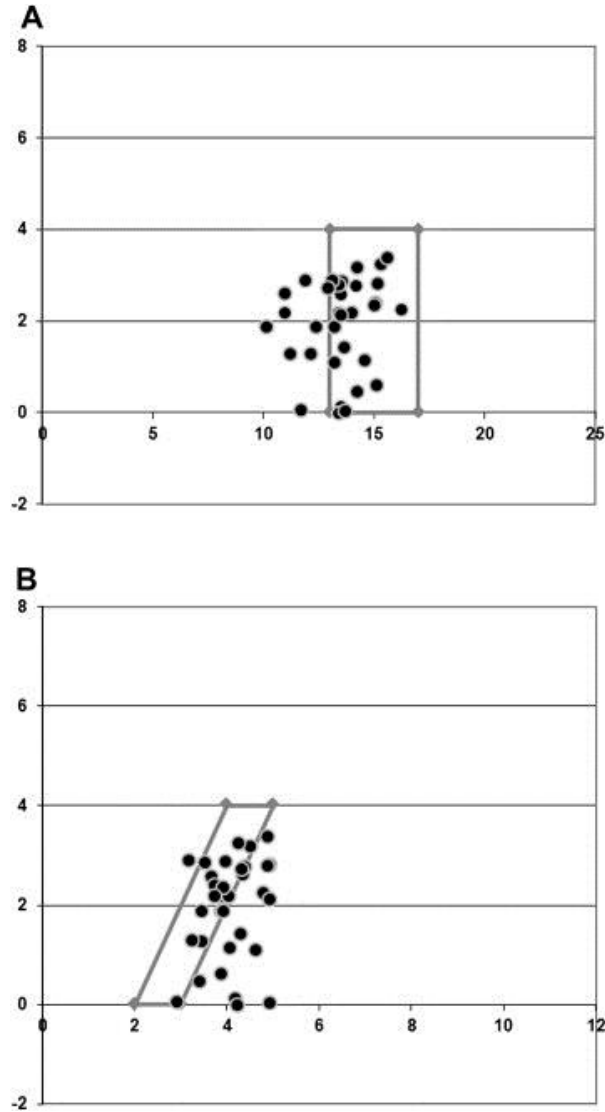
Figure 4. Locations of the center of "effective" contacts used for chronic high-frequency DBS determined during the clinical follow-up in the 20 patients (32 thalami). The coordinates are displayed on stereotactic diagrams; the inferior-superior direction (y-axis) is expressed in eighths of thalamus height (positive value above AC-PC; negative value below AC-PC): top, frontal view, laterality is expressed in mm (x-axis); bottom, lateral view, distance from PC (x-axis) is expressed in twelfths of AC-PC distance. The probabilistic location of Vim according to the proportional geometric scheme of Guiot et al. [9] modified by Benabid et al. [7] is shown for comparison (gray lines).

Follow-up and postoperative evaluations

Follow-up was performed at routine visits, usually every 3–6 months. Further minor adjustments of polarities, as well as benefits and adverse effects of Vim DBS were recorded at each visit. At these times, the UPDRS [21] Part III tremor item 21 and Fahn-Tolosa-Marin [22] clinical TRS were assessed. In patients with bilateral Vim implantation, tremor scores were evaluated on both sides.

Statistical analysis

Tremor scores at the last follow-up were compared with measurements before surgery. Pre- and postoperative scores were compared using the Wilcoxon signed-rank test. A P value of 0.05 was considered statistically significant. Statistical software SPPS (version 11.0, SPSS Inc.) was used for statistical analysis.

Results

Target localization based on MRI anatomic mapping

Vim was well delineated in all subjects. The shape, spatial orientation, and signal contrast of Vim as depicted on our 1.5-T WAIR images were similar to those observed on the Schaltenbrand and Bailey atlas [24], as well as in our 4.7-T MRI atlas [20] (Figs. 1 and 2). The hypointense band of Vim was clearly apparent, and well delineated on its posterior border by the hyperintense signal of the ventrocaudal nucleus (VC). Final outlining of Vim was achieved identifying the hypointense center median, dorsomedially, and the prelemniscal radiations (PLR) below, deeply hypointense, entering the thalamus on the posterior and ventral surface of Vim. The duration of the whole planning procedure for direct targeting was about 1 h and 30 min, including the determination of 14 structures for each thalamus (Fig. 2, Table 1).

MRI anatomy	Terminology according to Hassler R, Vogt C & Vogt O (in Schaltenbrand & Bailey, 1959)
Anteromedial	Anterior principalis or Anteroventralis
	Fasciculous
Anterolateral	Anterior medialis and Anterior inferior
	Anterior dorsalis
	Supranucleus lateropolaris
Dorsolateral	Dorsooralis
	Dorsointermedius
	possibly Dorso-caudalis
Dorsomedian	Dorsal superficialis
Intermediolateral	Zentrolateralis oralis
	Zentrolateralis intermedius
	Zentrolateralis caudalis
Ventro-oral	Ventrooralis anterior
	Ventrooralis medialis
	Ventrooralis internus
	Ventrooralis posterior
Ventrointermediate	Ventrointermedius
Ventrocaudal lateral	Ventrocaudalis anterior and posterior externus
	Ventrocaudalis parvocellularis externus
Ventrocaudal medial	Ventrocaudalis internus or Corpus Semilunare or Arcuate
	Ventrocaudalis parvocellularis internus
Medial	Medialis
Centre median	Centralis or Centre median
Parafascicular	Parafascicularis
Pulvinar	Pulvinaris or Posterior

Table 1. Structures outlined on 1.5-T MRI slices for the stereotactic planning. Thalamic nuclei are classified according to MRI anatomy [20]; the related terminology according to Hassler and Vogt [4] is given.

DBS electrode implantation

Between the two possible electrode tracts used for each hemisphere, the central one directed toward the target predetermined on stereotactic MRI for implantation of the DBS electrode was chosen for definitive implantation in 27 of 32 electrodes, that is, in 84.5% of cases. Intraoperative findings fitted with classical Vim behavior: kinesthetic neurons microrecordings when penetrating the nucleus and tremor arrest during macrostimulations [2,8,14]. The average

distance between the inferior border of Vim determined on WAIR imaging, and the final spot where was placed the contact after stimulation mapping, was 2.77 ± 2.6 mm (range 0–5.5 mm; SD = 2.1 mm). A second tract (medial or anterior tract) was required – and sufficient – in other cases (15.5%). The duration of the whole procedure of bilateral electrode implantation was about 6 h. No surgical complication was noticed. No hemorrhage was observed on postoperative CT-scan.

Location of electrode contacts used for continuous thalamic DBS

Among the 32 definitive electrodes implanted, 87.5% of contacts used for chronic thalamic DBS were located within the boundaries of Vim or intimately apposed to the caudal aspect of the nucleus, that is, where the hypointense PLR enter the thalamus, as depicted on WAIR images (Figs. 2A and 3C).

The mean coordinates of the "effective" contacts used for chronic thalamic DBS was 13.4 ± 1.5 mm lateral, 8.9 ± 1.5 mm anterior, and 4.11 ± 2.3 mm superior to PC. Marked variation in these values was noticed among the patients in the three planes. We observed significant differences, especially in the laterality and the anterior-posterior direction, between the effective contacts validated by postoperative outcomes on tremor control, and the probabilistic location of Vim (Fig. 4).

Postoperative evaluations

The UPDRS [21] Part III tremor item 21 and Fahn-Tolosa-Marin [22] clinical TRS were used to assess pre- and postoperative tremor (Table 2). The preoperative mean tremor score was 3.80 ± 0.30; after Vim DBS (last follow-up examination) the mean score dramatically reduced to 0.37 ± 0.75 in the stimulation-on state. The difference between pre- and postoperative tremor scores was statistically significant ($P < 0.01$). Adverse events observed during postoperative programming consisted in dysarthria for 4 patients and slight paresthesia for one patient. Usually, these symptoms disappeared with changes in stimulation parameters.

Tremor grades at UL[a] Clinical assessment		No. of implanted sides	
		Pre-Vim DBS	Post-Vim DBS
Parkinson's Disease (21 electrodes)			
UPDRS tremor item 21			
0	Absent	0	16
1	Slight, during action	0	4
2	Moderate, during action	0	1
3	Moderate, during posture handling and action	4	0
4	Severe, annoying for most activities	17	0
Essential Tremor (11 electrodes)			
Fahn-Tolosa-Marin TRS			
0	Absent	0	9
1	Slight, may be intermittent	0	0
2	Moderate (amplitude <2 cm)	0	1
3	Marked (amplitude 2–4 cm)	2	1
4	Severe (amplitude >4 cm)	9	0

Table 2. *Tremor grades pre- and post-Vim DBS in the 20 patients, according to disease type.*

Abbreviations: UL, upper limb; UPDRS, Unified Parkinson's Disease Rating Scale; TRS, tremor rating scale. [a] The results are related to the number of implanted sides, because, in bilaterally implanted patients, they may be different from one side to the other.

Discussion

Using a conventional 1.5-T MRI scanner, we used a dedicated stereotactic sequence (WAIR sequence) for enhancing direct detection capabilities of Vim within the thalamus. Qualitatively, at 1.5-T, the MRI anatomy of Vim is likely a less easy to interpret than those of STN and GPi [3,15–17]. However, WAIR sequence, combined with a high-field (4.7-T) MRI atlas [20] for comparison of multicontrast images and appropriate labeling, seems very helpful for direct visualization and targeting of Vim during stereotactic neurosurgery, as our result argues. Providing a significant enhancement of contrast between different gray matter territories, WAIR imaging reveals detailed intrathalamic structures that are readily distinguished from their surrounding, thus allowing clear delineation of the nuclei in question and providing internal architecture. The actual limit of the sequence is the voxel size, which depends on SNR, that impacts on the geometric resolution. However, the anatomic resolution of adjacent structures such as Vim and VC is noted to be dramatically enhanced compared with state-of-the-art Fast Spin Echo (FSE) T2-weighted images commonly used for stereotactic procedures. This thalamic sub-compartmentalization, based on multicontrast images analysis, matches the plates of the Schaltenbrand & Bailey atlas [24] and the slices of our 4.7-T MRI atlas [20]. On WAIR images, Vim is a hypointense band crossing the ventrolateral region of the thalamus. Vim is also darker than the surrounding nuclei in the atlas plates and in high-field MR microscopic images of the thalamus. Hence, clinical MRI anatomic mapping of the thalamus is feasible, as from 1.5-T MRI, based on the anatomic knowledge mastered from histological and high-field MRI data. The higher density of fibers within Vim than in VC [4] could explain the hypointense signal of Vim and the hyperintense signal of VC on WAIR images. This high density of fibers within Vim could also explain why Talairach et al. [23] did not identify Vim, which was mistaken for the PLR. The dense PLR are easy to identify on WAIR images, with a typical low hyposignal (Fig. 2), and enter the thalamus at the ventral and posterior region of Vim. Spielgelmann et al. [27] reported similar observations using a FSE sequence at 3-T. Hence, with the new acquisition technique described here, one can divide the ventral group of thalamic nuclei into different zones, delineated by their signal intensities and white matter bundles. The "pixelization" effect while increasing the scale (see Fig. 2) can lead discomfort for the user but does not change the anatomic

relationships, which are the pertinent parameters in order to identify structures. Voxels of $0.52 \times 0.62 \times 2$ mm3 used in our institution offer sharp enough boundaries between structures, enabling reliable planned trajectories as confirmed by the clinical results. Finally, our findings show that macroscopic MRI anatomic labeling is feasible in clinical conditions, using a 1.5-T WAIR sequence, even if structural abnormalities of gray matter and white matter in PD and ET, such as those recently described using diffusion tensor imaging [28,29], could have prevented or limited identification of anatomic structures.

To the best of our knowledge, this is the first study exploring the efficacy (clinical outcome on tremor), the duration of planning, and the safety (adverse events related to DBS, number of trajectories used to optimize DBS effects) of pure direct 3D stereotactic targeting of Vim in patients receiving thalamic DBS for disabling tremor. The success of DBS depends on accuracy in target determination. Till this day, Vim has remained the sole popular stereotactic target still requiring indirect methods for its targeting [7]. However, there are well-known limitations of classical stereotactic atlases, which limit their applications without technical precautions minimizing anatomical targeting errors. In the particular case of Vim, there are substantial individual variations in the location of basal ganglia and thalamic nuclei in humans [3,13,14]; and Vim is a small nucleus measuring approximately 2–4 mm anteroposteriorly, 7–10 mm dorsoventrally, and 4–6 mm mediolaterally [24]. Hence, although indirect methods work reasonably well, direct visualization of Vim is desirable to improve targeting of the electrodes during the first step, that is, the anatomic targeting. Improved first-step anatomic targeting is expected to reduce the number of electrode adjustments or tracts required to achieve ideal positioning, thus improving patient safety by decreasing the risk of hemorrhage and decreasing the procedure cost by shortening the surgery.

In our series, the central tract directed toward the target predetermined by MRI for implantation of the DBS electrode was chosen for definitive implantation in 84.5% of cases. In the remaining cases (15.5%), the second tract (medial or anterior) was used. Hence, improved MRI specifications with WAIR sequence and direct recognition of Vim appears helpful in targeting Vim, reducing the number of micro- and macroelectrode passes required to refine target location. Although authors have shown that Vim DBS without microelectrode recording also provided good clinical outcomes [30], intraoperative neurophysiology remains essential for a majority of

groups [7–9,31,32] to confirm the location of the electrode within Vim and to detect the presence of eloquent surrounding brain structures, such as VC or internal capsule. In the literature, of 3 centers reporting their results on microelectrode recording, one use 1 to 5 tracts (mean = 2.4 tracts) to adjust the tip position within Vim [31]; two others use the five-tract multi-electrode holder [7,32]. Hence, the ability of improved MRI to further reduce the number of brain penetrations – i.e., from 3 or more to 1 or 2 per side – appears greatly valuable.

In our study, 87.5% of contacts used for chronic thalamic DBS appeared to be located within the full height of Vim or intimately apposed to the caudal aspect of the nucleus, that is, where the hypointense PLR enter the thalamus. This latter area has been frequently included as an extension of the stereotactic targeting of Vim in surgery for the relief of tremor [9,27]. A non-negligible proportion of contacts were slightly more anterior and medial to the probabilistic Vim target (Fig. 4). Globally individual final target location varied using this representation likely because of interindividual anatomic differences, thus rendering direct visualization and targeting of Vim more reliable than indirect methods. Another explanation might be that the adjacent Ventral oral posterior (Vop) or center median/parafascicularis (CM-Pf) nuclei could also be appropriate targets for the relief of tremor [33,34], making the ventrolateral thalamus (i.e., Vim and Vop) and medial anatomic neighborhood of Vim more lenient to targeting errors.

The comparison of indirect and direct anatomic targeting techniques for electrode implantation, such as in Vim, cannot be done simply because the former is deterministic and the latter stochastic. Practically because the tremor's functional target seems rather wide (see above), the determination of the final functionally optimized spot for the placement of the electrode is broadly comparable using direct or indirect technique. In our series, this optimal spot was located within 2.77 ± 2.6 mm (range 0–5.5 mm) above the lower border of Vim, this value being comparable to the median 3D targeting adjustment of 2.9 mm (range 0–5.4 mm) reported with indirect targeting [31]. These data suggest that MRI anatomic mapping may be helpful in determining Vim anatomy. We would like to emphasize that the endpoint of the optimized anatomic trajectory was not considered as the "stereotactic Vim target point", but instead as an anatomical landmark (i.e., the lower border of Vim) allowing planning electrophysiological mapping along the longest axis of the nucleus. The optimal spot where we observed the best intraoperative stimulation parameters was located on average 2.77 mm above the lower border of

Vim. However, for each individual, this optimal spot could be found between this lower border where PRL enters (0 mm) and the superior region of Vim (5.5 mm).

To summarize, direct anatomic targeting could be of interest in the near future, because it can reduce the number of trajectories and allows the exploration of Vim along its longest axis (as shown in Fig. 3), thus increasing the chance to find the best functional site for electrode placement, often located in the intermediate part (transversally) of Vim supporting the forelimb control [8]. Our clinical outcomes are consistent with studies that have established the efficacy of Vim DBS for the symptomatic treatment of ET or the tremor associated with PD [30,35,36]. Thus, the present study demonstrates that 1.5-T MRI with WAIR sequence enables accurate treatment planning by direct visualization of the targeted Vim.

Since the recent introduction of electric field simulation in neuromodulation, it is of upmost importance to explore the anatomy of each individual. To date, probabilistic stimulation atlas has been used to analyze DBS within the subthalamic region [37]. We assume that the simulation of electric field according to each individual data should likely be an important step forward. Thus, affordable individual 3D MRI anatomy of the thalamus, as provided with our approach, could enable to better master the subtle biophysical mechanism of DBS. Additionally, such a detailed patient-specific 3D model of the target area could facilitate postoperative programming and the interpretation of stimulation-induced side effects by highlighting a comprehensive 3D anatomic relationship between the DBS electrode, the targeted nucleus, and its surrounding structures.

Beyond direct targeting for thalamic DBS procedures, the theoretical implications of our study are important. Direct visualization of Vim is an anatomic, individual-based approach that exempt from uncertainty in stereotactic atlases. Therefore, it allows an accurate stereotactic surgical navigation making more conceivable the use of radiosurgery as an option for the production of thalamic lesions in patients not eligible for DBS or radiofrequency thalamotomy. Gamma-Knife thalamotomy have already proven its effectiveness for long-term control of ET [38]. Nonetheless, the obvious drawback with radiosurgery is the destructive and irreversible nature inherent to the method, which can lead to permanent complications [38]. Therefore, a precise preoperative planning for target selection is critical. On the basis of a reliable MRI anatomical mapping, as describe in our study, a precise radiosurgical lesion involving the whole Vim, and a more accurate dosimetry could be affordable.

Financial disclosures

Acknowledgments

References

[1] G. Guiot, P. Derome The principles of stereotaxic thalamotomy E.A. Kahn, E.C. Crosby, R.C. Schneider, J. Taren (Eds.), Correlative neurosurgery, Charles C Thomas, Springfield (1969), pp. 376-401

[2] L.V. Laitinen Brain targets in surgery for Parkinson's disease. Results of a survey of neurosurgeons J Neurosurg, 62 (1985), pp. 349-351

[3] H. Hirabayashi, M. Tengvar, M.I. Hariz Stereotactic imaging of the pallidal target Mov Disord, 17 (Suppl. 3) (2002), pp. 130-134

[4] R. Hassler Anatomy of the thalamus G. Shaltenbrandt, P. Bailey (Eds.), Introduction to stereotaxis with an atlas of the human brain, Georg Thieme-Verlag, Stuggart (1959), pp. 230-290

[5] T. Hirai, E.G. Jones A new parcellation of the human thalamus on the basis of histochemical staining Brain Res Rev, 14 (1989), pp. 1-34

[6] Y. Shinoda, T. Futami, S. Kakei Input-output organization of the ventrolateral nucleus of the thalamus Stereotact Funct Neurosurg, 60 (1993), pp. 17-31

[7] A.L. Benabid, A. Koudsie, A. Benazzouz, J.F. Le Bas, P. Pollak Imaging of subthalamic nucleus and ventralis intermedius of the thalamus Mov Disord, 17 (Suppl. 3) (2002), pp. 123-129

[8] A.L. Benabid, P. Pollack, D. Gao, D. Hoffman, P. Limousin, E. Gay, et al. Chronic electrical stimulation of the ventralis intermedius nucleus of the thalamus as a treatment of movement disorders J Neurosurg, 84 (1996), pp. 203-214

[9] G. Guiot, P. Derôme, J.C. Trigo Le tremblement d'attitude. Indication la meilleure de la chirurgie stéréotaxique Press Med, 75 (1967), pp. 2513-2518

[10] R. Spiegelmann, W.A. Friedmann Rapid determination of thalamic CT-stereotactic coordinates: a method Acta Neurochir (Wien), 110 (1991), pp. 77-81

[11] A. Machado, A.R. Rezai, B.H. Kopell, R.E. Gross, A.D. Sharan, A.L. Benabid Deep brain stimulation for Parkinson's disease: surgical technique and perioperative management Mov Disord, 21 (Suppl. 14) (2006), pp. 247-258

[12] S.E. Hua, I.M. Garonzik, J.I. Lee, F.A. Lenz Thalamotomy for tremor D. Tarsy, J.L. Vitek, A.M. Lozano (Eds.), Surgical treatment of Parkinson's disease and other movement disorders, Humana Press, Totowa, NJ (2002), pp. 99-114

[13] J.B. Brierley, E. Beck The significance in human stereotactic brain surgery of individual variation in the diencephalons and globus pallidus J Neurosurg Psychiatry, 22 (1959), pp. 287-298

[14] P.J. Kelly, P. Derome, G. Guiot Thalamic spatial variability and the surgical results of lesions placed with neurophysiologic control Surg Neurol, 9 (1978), pp. 307-315

[15] J.J. Lemaire, J. Coste, L. Ouchchane, F. Caire, C. Nuti, P. Derost, et al. Brain mapping in stereotactic surgery: a brief overview from the probabilistic targeting to the patient-based anatomic mapping NeuroImage, 37 (Suppl. 1) (2007), pp. 109-115

[16] J. Lemaire, J. Coste, L. Ouchchane, S. Hemm, P. Derost, M. Ulla, et al. MRI anatomical mapping and direct stereotactic targeting in the subthalamic region: functional and anatomical correspondence in Parkinson's disease IntJCARS, 2 (2) (2007), pp. 75-85

[17] V.A. Magnotta, S. Gold, N.C. Andreasen, J.C. Ehrhardt, W.T. Yuh Visualization of subthalamic nuclei with cortex attenuated inversion recovery MR imaging NeuroImage, 11 (2000), pp. 341-346

[18] S.C. Deoni, B.K. Rutt, A.G. Parrent, T.M. Peters Segmentation of thalamic nuclei using a modified k-means clustering algorithm and high-resolution quantitative magnetic resonance imaging at 1.5 T NeuroImage, 34 (2007), pp. 117-126

[19] J.J. Lemaire, F. Caire, J.M. Bony, J.L. Kemeny, A. Villeger, J. Chazal Contribution of 4.7 Tesla MRI in the analysis of the MRI anatomy of the human subthalamic area Acta Neurochir (Wien), 146 (2004), pp. 906-907

[20] J.J. Lemaire, L. Sakka, L. Ouchchane, F. Caire, J. Gabrillargues, J.M. Bonny Anatomy of the human thalamus based on spontaneous contrast and microscopic voxels in high-field magnetic resonance imaging Neurosurgery, 66 (Suppl. 3 Operative) (2010), pp. 161-172

[21] S. Fahn, R.L. Elton, UPDRS Programm Members Unified Parkinson's disease rating scale S. Fahn, C.D. Marsden, M. Goldstein, D.B. Calne (Eds.), Recent developments in Parkinson's disease, vol. 2, Macmillan Healthcare Information, Florham Park, NJ (1987), pp. 153-163

[22] S. Fahn, E. Tolosa, C. Martin Clinical rating scale for tremor J. Jancovic, E. Tolosa (Eds.), Parkinson's disease and movement disorders (2nd ed.), William & Wilkins, Baltimore (1993), pp. 271-280

[23] J. Talairach, G. Szikla, P. Tournoux, A. Prosalentis, M. Bornas-Ferrier (Eds.), Atlas d'anatomie stéréotaxique du télencéphale, Masson, Paris (1967)

[24] G. Schaltenbrand, P. Bailey (Eds.), Introduction to stereotaxis with an atlas of the human brain, Georg Thieme Verlag, Stuttgart (1959)

[25] A. Morel, M. Magnin, D. Jeanmonod Multiarchitectonic and stereotactic atlas of the human thalamus J Comp Neurol, 387 (1997), pp. 588-630

[26] S. Hemm, J. Coste, J. Gabrillargues, L. Ouchchane, L. Sarry, T. Caire, et al. Contact position analysis of deep brain stimulation electrodes on post-operative CT images Acta Neurochir (Wien), 151 (2009), pp. 823-829

[27] R. Spiegelmann, O. Nissim, D. Daniels, A. Ocherashvilli, Y. Mardor Stereotactic targeting of the ventrointermediate nucleus of the thalamus by direct visualisation with high-field MRI Stereotact Funct Neurosurg, 84 (2006), pp. 19-23

[28] G. Gattellaro, L. Minati, M. Grisoli, C. Mariani, F. Carella, M. Oslo, et al. White matter involvement in idiopathic Parkinson's disease: a diffusion tensor imaging study Am J Neuroradiol, 30 (2009), pp. 1222-1226

[29] D.H. Shin, B.S. Han, H.S. Kim, P.H. Lee Diffusion tensor imaging in patients with essential tremor Am J Neuroradiol, 29 (2008), pp. 151-153

[30] P. Blomstedt, G.M. Hariz, M.I. Hariz, L.O. Koskinen Thalamic deep brain stimulation in the treatment of essential tremor: a long-term follow-up Br J Neurosurg, 21 (2007), pp. 504-509

[31] R.L. Alterman, G.T. Reiter, J. Shils, B. Skolnick, J.E. Arle, M. Lesutis, et al. Targeting for thalamic deep brain stimulator implantation without computer guidance: assessment of targeting accuracy Stereotact Funct Neurosurg, 72 (1999), pp. 150-153

[32] D. Dormont, P. Cornu, B. Pidoux, A.M. Bonnet, A. Biondi, C. Oppenheim, et al. Chronic thalamic stimulation with three-dimensional MR stereotactic guidance AJNR Am J Neuroradiol, 18 (1997), pp. 1093-1107

[33] H. Bjartmarz, S. Rehncrona Comparison of accuracy and precision between frame-based and frameless stereotactic navigation for deep brain stimulation electrode implantation Stereotact Funct Neurosurg, 85 (2007), pp. 235-242

[34] D. Caparros-Lefebvre, S. Blond, M.P. Feltin, P. Pollack, A.L. Benabid Improvement of levodopa induced dyskinesias by thalamic deep brain stimulation is related to slight variation in electrode placement: possible involvement of the centre median and parafascicularis complex J Neurol Neurosurg Psychiatry, 67 (1999), pp. 308-314

[35] A.L. Benabid, P. Pollak, A. Louveau, S. Henry, J. de Rougemont Combined (thalamotomy and stimulation) stereotactic surgery of the Vim thalamic nucleus for bilateral Parkinson disease Appl Neurophysiol, 50 (1987), pp. 344-346

[36] J.G. Pilitsis, L.V. Metman, J.R. Toleikis, L.E. Hughes, S.B. Sani, R.A. Bakay Factors involved in long-term efficacy of deep brain stimulation of the thalamus for essential tremor J Neurosurg, 109 (2008), pp. 640-646

[37] C.R. Butson, S.E. Cooper, J.M. Henderson, B. Wolgamuth, C.C. McIntyre Probabilistic analysis of activation volumes generated during deep brain stimulation Neuroimage, 54 (2011), pp. 2096-2104

[38] R.F. Young, F. Li, S. Vermeulen, R. Meier Gamma knife thalamotomy for treatment of essential tremor: long-term results J Neurosurg, 112 (2010), pp. 1311-1317